Fuel 242 (2019) 109–123

Contents lists available at ScienceDirect

Fuel

journal homepage: www.elsevier.com/locate/fuel

Full Length Article

Experimental study of the spray collapse process of multi-hole gasoline fuel injection at flash boiling conditions

Shengqi Wu[a,*], Shangze Yang[b], Margaret Wooldridge[a], Min Xu[b,*]

[a] Department of Mechanical Engineering, University of Michigan, Ann Arbor, MI 48109, USA
[b] School of Mechanical Engineering, National Engineering Laboratory for Automotive Electronic Control Technology, Shanghai Jiao Tong University, Shanghai 200240, China

ARTICLE INFO

Keywords:
Gasoline direct injection
Multi-hole injector
Flash boiling
Spray imaging
Structure and pattern
Spray collapse

ABSTRACT

In this study, fuel sprays of a 1-hole injector and a 6-hole injector were investigated under a wide range of subcooled and flash-boiling conditions using high-speed imaging in a constant-volume spray chamber. The fuel pressure was held constant at 15 MPa, and the fuel temperature was varied from 25 °C to 85 °C. Ambient pressure in the spray chamber was varied from 20 kPa to 200 kPa and the chamber temperature was held constant at 25 °C. The results show decreasing ambient pressure led to flash boiling for sprays from the 1-hole injector and consequently enhanced fuel atomization; however, the spray processes of the multi-hole injector were not well represented by the single-hole injector when considering spray collapse. For the 6-hole injector, the results showed plume interaction was more important than chamber density in controlling the spray characteristics. Specifically, expanded fuel plumes induced by flash boiling increased interaction between adjacent fuel plumes and consequently affected the spray structure. Slight plume interaction resulted in moderate spray collapse, shorter spray penetration and wider spray angles. Strong plume interaction triggered severe spray collapse, leading to longer spray penetration and smaller spray angles. Plume interaction started in the near nozzle region, and sustained interaction depended on the injector configuration and the superheat degree. At strong flash-boiling conditions (where the ratio of the ambient pressure to the fuel saturation pressure was less than 0.3), plume interaction increased with time and as the spray moved downward away from the nozzle exit due to fast fuel atomization and evaporation. The potential for spray collapse of a multi-hole injector was primarily attributed to the effects of the fuel properties, injector configuration and operating conditions (e.g. ambient pressure, fuel temperature and pressure, etc.) on the development of the plume width relative to changes in the distance between adjacent plumes. Adjusting the parameters to increase the distance between adjacent fuel plumes or decrease plume width, will decrease plume interaction and spray collapse can be suppressed, and vice versa.

1. Introduction

Flash-boiling fuel sprays are important and timely research topics related to cleaner combustion of internal combustion (IC) engines. Flash-boiling fuel sprays can improve fuel economy and reduce particulate mass and particulate number emissions [1–4], especially under engine cold start conditions [3,4]. Flash-boiling sprays can finely atomize fuel even at very low fuel pressure, which removes the need for an expensive and complex high-pressure fuel system. Fuel boiling, which produces a considerable amount of bubbles inside the liquid core, improves spray atomization [5–7] and evaporation [8–12] significantly, and consequently enhances air entrainment [13] and fuel and air mixing [4]. Internal flow studies of flash-boiling fuel sprays showed fuel bubbles were generated along the inside of the nozzle wall before the fuel was injected into the combustion chamber [14–17], and the fuel bubbles promoted the spray primary breakup process remarkably [16–21]. The thermo-physical properties of a fuel such as saturation temperature, latent heat of vaporization, surface tension, density and viscosity are the key parameters to determine the atomization and evaporation process [22,23]. In addition, the presence of flash-boiling bubbles in the nozzle can improve the end-of-injection characteristics by eliminating large drops or ligaments, which could eliminate issues with injector deposits caused by trapped liquid fuel in the nozzle at the end of injection [20,24]. However, the physical features of flash-boiling sprays change with the superheat degree [25–27]. For example, under flare flash-boiling conditions, fuel sprays from multi-hole injectors can

* Corresponding authors.
E-mail addresses: shengqiwu@gmail.com (S. Wu), mxu@sjtu.edu.cn (M. Xu).

https://doi.org/10.1016/j.fuel.2019.01.027
Received 6 October 2018; Received in revised form 1 January 2019; Accepted 3 January 2019
Available online 07 January 2019
0016-2361/

Nomenclature

ASOF	after the start of fueling
$D(H)$	distance between center points of two adjacent fuel plumes at the H cross-sectional plane
GDI	gasoline direct injection
H	distance from the injector tip to the cross-sectional plane of interest
n	number of nozzles in the injector
P_a	ambient pressure
P_s	fuel saturation vapor pressure
P_a/P_s	dimensionless superheat degree
R	distance between the plume centerline and the injector centerline
$W(H)$	width of the plumes at the H cross-sectional plane
α	angle between two adjacent plumes
δ	correction factor representing the effects of ambient gas motion and other external flow on the change in the distance between adjacent fuel plumes
ΔD	change in the distance between two adjacent fuel plumes at times t_1 and t_2
ΔW	change in the plume width between time t_1 and t_2
θ	drill angle of each nozzle

collapse to the centerline of the spray, altering the spray structure [25–27], which alters the direction of the spray (i.e. the spray targeting) and the fuel distribution in the combustion chamber [28,29]. As the superheat degree reduces to a certain level, the spray geometry is no longer dominated by the injector configuration, and regardless of injector configuration and type, collapsed fuel spray structures with one fuel plume are formed at strong flash-boiling conditions [30–32]. Generally, severely collapsed fuel sprays have longer spray penetration distances and smaller spray angles compared with sprays that have not collapsed. Therefore, there is disagreement whether flash boiling is beneficial or harmful to mixing and ultimately engine performance. Xu et al. [3] found even when severe collapse of the fuel spray occurred, fuel economy was improved and total hydrocarbon, carbon monoxide and particulate number emissions were reduced in a study using a single-cylinder optically-accessible spark-ignition direct-injection (SIDI) engine. But Schulz et al. [29] confirmed increasing the fuel temperature did not lead to a constant reduction of the wall film. Rather, severely collapsed flash-boiling sprays led to an accumulation of the wall film mass in a small area, which required much longer time for evaporation. The key point of this argument lies in whether the deformed spray structure that occurs due to flash boiling is suitable for the specific combustion system. However, combustion system design and optimization are based on conventional liquid fuel spray characteristics, and consideration of the effects of flash boiling are not typically considered. In addition, the characteristics during transition from conventional spray behavior to flash boiling are complex, not well understood, difficult to control, and are very sensitive to fuel temperature and ambient pressure. The lack of quantitative information on flash boiling of fuel sprays and on the transition from conventional spray behavior to flash-boiling behavior is the motivation for this work.

Several studies have advanced our understanding of the mechanisms controlling flash boiling fuel sprays and the characteristics of collapsed sprays. Zeng et al. [25] found the dimensionless superheat degree P_a/P_s, which was defined as the ratio of the ambient pressure (P_a) to the fuel saturation vapor pressure (P_s), was effective to characterize the overall geometry of flash-boiling sprays. Fuel plumes of adjacent nozzles started interacting when P_a/P_s was between 0.3 and 1.0, and the interactions resulted in shorter spray penetration and wider spray angle. However, the spray structure of the multi-hole injector collapsed to the spray centerline when P_a/P_s was less than 0.3. These severely collapsed fuel sprays in this region exhibited longer penetration and smaller spray angles. Contrary to the study by Zeng et al. [25], Lacey et al. [28] found the dimensionless P_a/P_s value was not as effective at capturing the point of spray collapse of flash-boiling sprays, especially of different fuels. It was showed when the dimensionless P_a/P_s ratios were comparable between a heavy fuel injected into high vacuum conditions and a light fuel injected into much denser conditions, considerable differences in the spray penetration were observed, especially when there was a large difference in the boiling point of the two fuels [28]. In addition, an injector with a larger cone angle required stronger superheat degree, i.e., a smaller P_a/P_s value, to produce collapsed fuel sprays [28]. Similarly, Mojtabi et al. [33] found that fuel spray of an injector with 60° nominal angle underwent more severe collapsed behavior than the fuel spray of an injector with a 90° nominal angle. Other studies have found higher fuel pressure can suppress plume interaction and consequently spray collapse [26,29,34]. From the research of Aleiferis et al. [19], spray collapse was thought to be induced by vaporized fuel being drawn to the low pressure core of the spray between the closely spaced plumes. Wu et al. [24,31] thought in-nozzle fuel evaporation which altered the direction of the fuel at the nozzle exit was responsible for spray collapse of a 1-slot injector, and ambient gas motion triggered by a pressure differential resulted in spray collapse of multi-hole injectors. Li et al. [35] concluded the spray collapse of a multi-hole injector was due to vapor condensation, which was caused by a decrease in liquid temperature and an increase in local static pressure.

The previous studies show the conditions which lead to spray collapse and the characteristics of flash-boiling fuel sprays are affected by fuel temperature, fuel pressure, injector configuration, fuel properties, ambient gas density and pressure. De-convolving the effects of these parameters on the structure of and transition to flash-boiling sprays is challenging, and flash-boiling spray models have not converged to consensus theory on the mechanisms by which these parameters affect fuel sprays [36]. Moreover, modeling approaches often differentiate between considering internal or external flow fields. Some flash-boiling spray models focus on the near-field region outside the nozzle [37,38] and others on the superheated flows inside the nozzle [39–41].

Additional understanding of the fundamental mechanisms and features of flash-boiling sprays is vital to enabling the application of flash boiling in modern IC engines. Fundamental experimental studies of flash-boiling sprays are particularly well suited to the development of flash-boiling spray theory as a large parametric space can be considered, including the transition from conventional spray behavior to flash-boiling spray behavior. To address this need, experimental studies of a 1-hole injector and a 6-hole injector were conducted to investigate and compare the spray collapse processes. A wide range of subcooled and flash-boiling conditions were investigated. First, effects of spray collapse on axial spray structures of the 6-hole injector were considered, followed by analysis of high-speed spray pattern images at various cross-sectional planes. The results are discussed in the context of the dimensionless superheat degree and parameters defining conditions of collapse are proposed.

2. Experimental information

2.1. Experimental setup

Two kinds of experimental methods were used in this research: high-speed backlit imaging and high-speed radial laser imaging. The high-speed backlit imaging system was applied to capture the macroscopic axial spray structure, and the high-speed radial laser imaging technique was used to record cross-sectional spray patterns at various

planes downstream of the injector tip. Fig. 1 shows a schematic of the high-speed backlit imaging system. A high-power xenon lamp was used as the source for backlighting, and the fuel spray imaging was captured using a high-speed camera. The camera was Phantom V7.3, and worked at 10 k frame rate with pixel resolution of 544x560. A constant volume chamber (CVC) with inner diameter of 200 mm was used to produce various ambient pressures. There were four optical accessible windows of the CVC, of which there were two circular windows with the optical diameter of 100 mm and two rectangular optical windows with the dimension of 20 mm in width and 100 mm in height. Quartz was used as the material of the optical windows. Pressure in the CVC was measured at the lower part using a transducer with an uncertainty of 0.25% at full scale of 5 MPa. A high-pressure nitrogen cylinder and a vacuum pump were connected to the CVC for pressure conditions higher than 0.101 MPa and vacuum, respectively. Compressed high-pressure nitrogen was applied to actuate the accumulator by pumping the liquid fuel inside the accumulator to a target pressure below 20 MPa. During the test, pure nitrogen flushed the CVC continuously to remove residual fuel for clear spray images. The injector was mounted on the top of the CVC. The fuel temperature was controlled via a heat exchanger which provided continuous coolant flows through a water jacket around the injector. The temperature between the coolant and the fuel was calibrated via an injector embedded with a thermal couple in the sac. Synchronization between the injector actuation and the camera recording was realized via a digital pulse generator, which could produce several triggering signals with precisely controlled offset of 1 μs.

A high-speed radial laser imaging system was used with the same CVC setup to record the spray patterns at various distances downstream of the injector tip. Fig. 2 shows a schematic of the radial imaging system. The ambient pressure, fuel pressure and fuel temperature control systems were the same as those used with the high-speed backlit imaging system. A Nd:YLF laser with a laser wavelength of 527 nm (22 mJ @1000 Hz) and a pulse repetition rate of 10 kHz was applied to illuminate the fuel spray. A high-speed camera equipped with a band-pass filter (with central wavelength of 527 nm) was used to capture the fuel spray patterns. The high speed camera was Phantom V1210, and worked at 10 k frame rate with pixel resolution of 896x800. During the test, various spacers between the injector fixture and CVC were used to adjust the distance between the injector tip and imaging plane, by which the spray pattern at various distances downstream of the injector tip could be recorded with the same resolution and scale. The distance between the injector tip and imaging plane varied from 10 mm to 70 mm with increments of 10 mm.

2.2. Injector configuration

Two injectors were considered in this study: a 1-hole injector and a 6-hole injector. Fig. 3 shows the nozzle configuration of the two injectors. For the 6-hole injector, the nozzles each had the same structure and were evenly distributed in the injector tip. The 1-hole injector was created by masking the other 5 nozzles of the 6-hole injector. The nozzle length-to-diameter ratio was 1.5. Each nozzle was a step hole with an inner diameter of 0.2 mm and length of 0.3 mm, and the diameter of the counter bore was 0.4 mm. The drill angle of each nozzle was 30°.

2.3. Experimental parameters

Table 1 presents the test parameters of the study. N-hexane was chosen as the test fuel. Fuel pressure and the ambient temperature were constant at 15 MPa and 23 °C, respectively. Injection duration was fixed at 1.5 ms. Fuel temperature varied from 25 °C to 85 °C, and ambient pressure varied from 20 kPa to 200 kPa, which produced a wide range of subcooled and superheated conditions. Fig. 4 plots the vapor pressure of n-hexane and the ambient chamber pressures and fuel temperatures considered in this study. The test conditions above the vapor pressure of n-hexane are subcooled conditions, and the test conditions below the vapor pressure of n-hexane are superheated conditions. Conditions well below the vapor pressure curve are stronger superheated conditions. Table 2 presents the dimensionless superheat degrees, P_a/P_s, of each

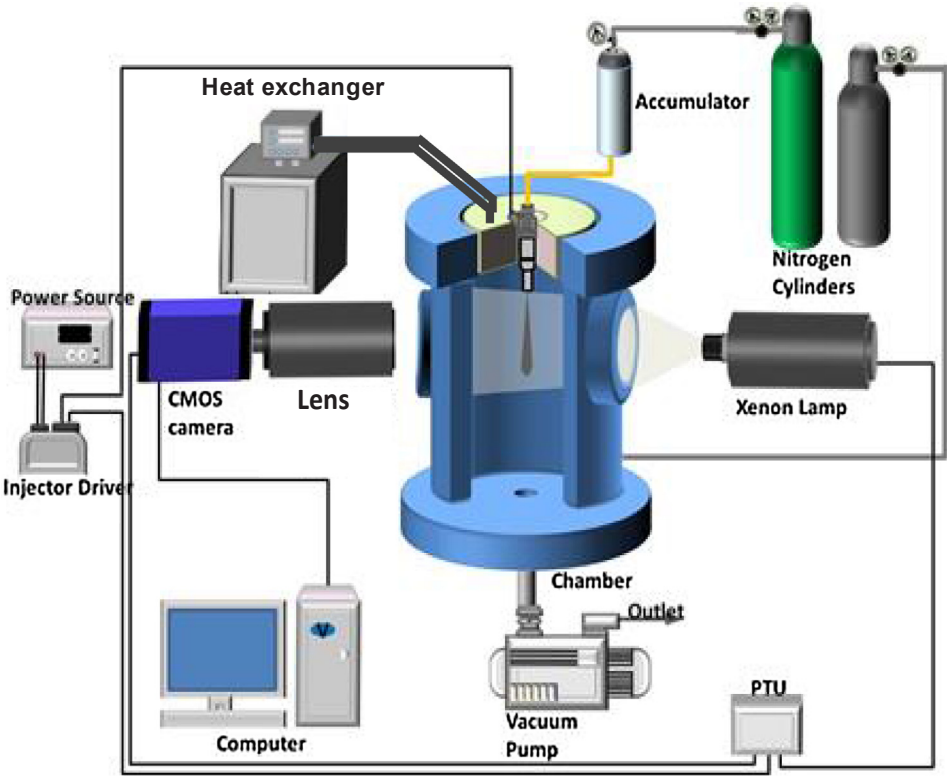

Fig. 1. Experimental setup of the high-speed backlit imaging system.

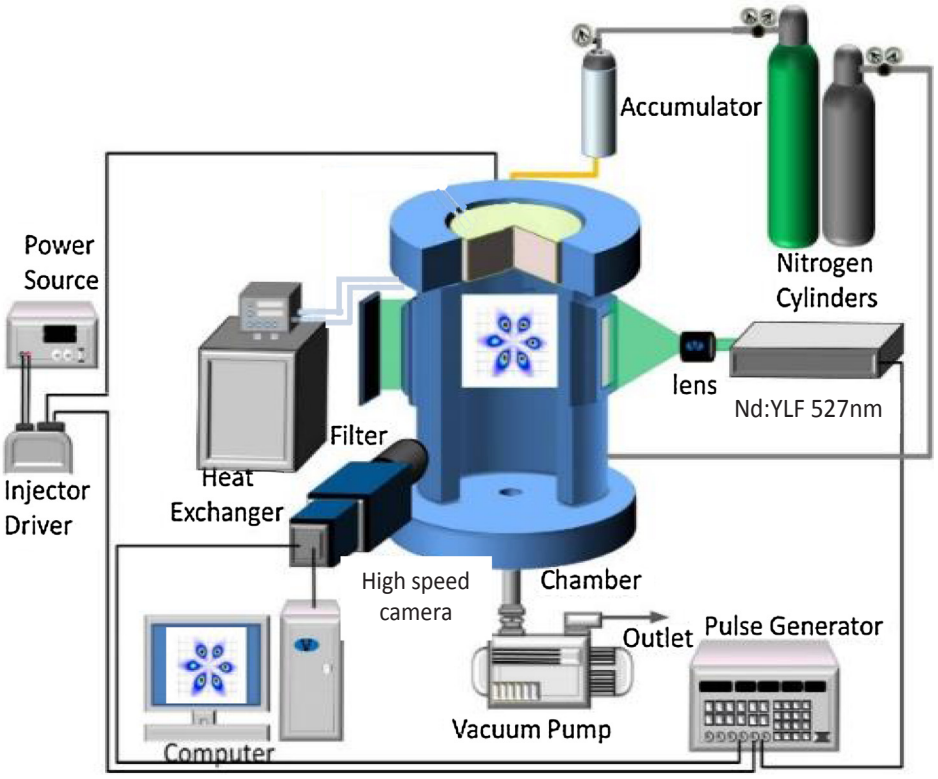

Fig. 2. Experimental setup of the high-speed laser radial imaging system.

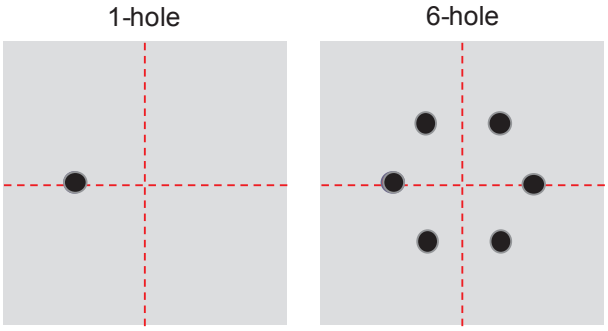

Fig. 3. Nozzle configuration of test injectors.

Table 1
Test parameters.

Parameter	Specification
Fuel	n-hexane
Fuel pressure (MPa)	15
Fuel temperature (°C)	25 to 85
Ambient pressure (kPa)	20 to 200
Ambient temperature (°C)	23 ± 2
Injection duration (ms)	1.5

test condition in the study. When P_a/P_s is larger than 1, the fuel is subcooled and the result is a liquid fuel spray. When P_a/P_s is between 0.3 and 1, the spray is at transitional flash-boiling conditions. When P_a/P_s is less than 0.3, the fuel is superheated and the result is a flash-boiling spray.

2.4. Spray image post-processing procedure

In this study, backlit spray images have very high signal-to-noise ratios, and spray penetration of macroscopic spray images were

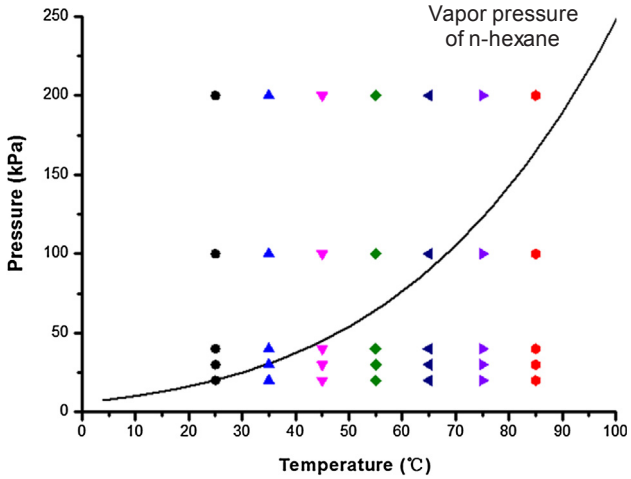

Fig. 4. Comparison of ambient pressure and fuel temperature conditions with the vapor pressure of the test fuel, n-hexane.

Table 2
Test conditions and corresponding values of dimensionless superheat degree, P_a/P_s. The borders between flare flash-boiling ($P_a/P_s < 0.3$), transitional flash-boiling ($0.3 \le P_a/P_s \le 1$) and subcooled ($P_a/P_s > 1$) conditions are emphasized with thicker lines.

P_a/P_s \ T_f(°C) / P_a(kPa)	25	35	45	55	65	75	85
20	1.0	0.67	0.44	0.3	0.22	0.16	0.12
30	1.5	1.0	0.67	0.46	0.33	0.25	0.18
40	2.0	1.33	0.89	0.62	0.44	0.33	0.24
100	5.0	3.33	2.22	1.54	1.11	0.82	0.61
200	10.0	6.66	4.44	3.08	2.22	1.64	1.23

analyzed for quantitative comparisons. Spray penetration was defined as the longest vertical distance from the leading edge of the spray boundary to the injector tip and the definition is shown in Fig. 5 for typical backlit spray images. Post-processing of the macroscopic spray images consisted of background subtraction, thresholding and binarization. The threshold value was defined as 5% of the highest intensity of each spray image. The image post-processing was conducted using Matlab. Spray pattern images were used for qualitative evaluation of the morphology of the spray collapse process, and no quantitative metrics were derived from the spray pattern images.

3. Results and discussions

In this section, the results for the spray imaging of the axial spray structure of the 1-hole injector and the 6-hole injector are presented, followed by the results for the spray patterns of the 6-hole injector at various cross-sectional planes. The data sets are discussed in the context of the effects of fuel temperature and ambient pressure on the spray features. The characteristics of plume interactions and the effects of plume interaction on spray collapse are identified. At the end of the section, observations from the current work are combined with results in the literature to discuss the trends of the effects of injection parameters, i.e., injector physical configuration, fuel pressure, fuel properties and ambient conditions, on plume interaction and spray collapse.

3.1. Axial spray analysis of 1-hole injector

The single-hole injector results provide a baseline for comparison with the multi-hole injector results. Fig. 6 shows spray image sequences of the 1-hole injector at fuel temperatures of 25 °C and 85 °C and ambient pressures from 20 kPa to 200 kPa, where the time corresponds to the time after the start of fueling (ASOF). Fig. 6(a) shows the results for fuel temperature of 25 °C and $P_a/P_s > 1.0$; corresponding to subcooled conditions. Fig. 6(b) shows results where P_a/P_s was less than one for all ambient pressures except $P_a = 200$ kPa. The images in Fig. 6(a) show the spray structures at 200 kPa and 100 kPa ambient pressures were more compact than for lower ambient pressures. The compact structures are due to the increase in ambient gas density associated with the higher ambient pressures. Similar qualitative changes were observed at the higher fuel temperature, as seen in Fig. 6(b), but to a lesser extent.

Comparing Fig. 6(a) and (b) at the ambient pressure of 200 kPa, the spray structures were very similar. The small effect of fuel temperature at 200 kPa on the spray structure is attributed to the small change (7.4%) in fuel density associated with increasing the fuel temperature from 25 °C to 85 °C. However, when the ambient pressure was lower than 100 kPa, the injection conditions became superheated, with the lowest value of dimensionless superheat degree at 20 kPa ambient pressure where $P_a/P_s = 0.12$. (Recall, the lowest value of P_a/P_s corresponds to the highest levels of superheating.) At 20 kPa the spray structures were different between the two fuel temperatures. Enhanced spray atomization was observed when the fuel temperature was 85 °C due to flash-boiling effects. Fractal structures and small fuel drops around the spray tip were also detected (at higher magnification than the images shown in Fig. 6). Small vortices could also be seen near the upper and lower part of the spray tip when the ambient pressure was 30 kPa and 20 kPa for the fuel temperature of 85 °C.

Fig. 7 shows the average spray penetration as a function of time corresponding to the results presented in Fig. 6. For each set of experimental conditions, 20 injection cycles were recorded and the error bars in the figure represent the standard deviation of the data. As expected, the rate of spray penetration decreased at the highest ambient pressures for both fuel temperatures. As seen in Fig. 7(a) when the fuel temperature was 25 °C and at early times (e.g. 0.1 ms ASOF), there was little difference in the spray penetration data at the different ambient pressures. This is attributed to the high fuel pressure used in the study. According to the work by Hiroyasu et al. [42], spray penetration during the primary breakup stage is governed by the fuel density and the difference between the fuel pressure and the ambient pressure. Although the ambient pressure changed significantly in these experiments, the effect on the pressure differential was negligible due to the high fuel pressure. Therefore, the ambient pressure had almost no impact on spray penetration during the early stage of the spray development. In the secondary breakup region, spray penetration is influenced by the pressure differential, the ambient gas density, and the nozzle diameter [42]. Large changes in the ambient pressure lead to substantial ambient density changes, and consequently large differences in spray penetration. As observed in Fig. 7, higher ambient pressures resulted in higher ambient gas density, and subsequently smaller spray penetration distances for both fuel temperatures. However, for Fig. 7(b) when the fuel temperature was 85 °C, almost identical spray penetration was observed at early times (e.g., < 0.3 ms ASOF) at the different ambient pressures. Decreasing the ambient pressure reduces the air drag forces on the spray (increasing penetration), but lower ambient pressure also increases the level of superheating. Stronger superheating

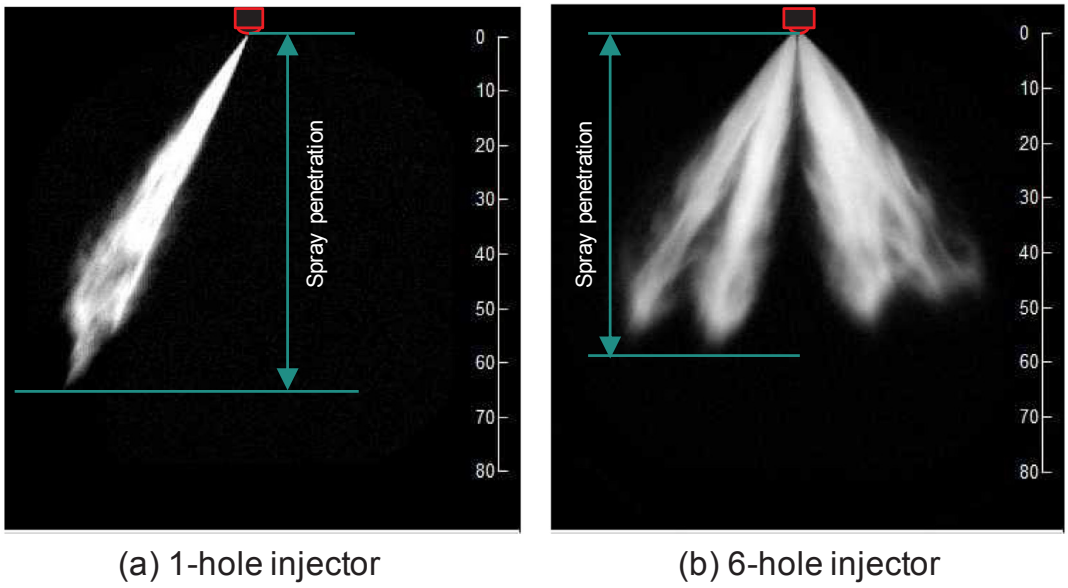

Fig. 5. Images showing the definitions used to quantify the penetration distance of the single hole and multi-hole injector sprays.

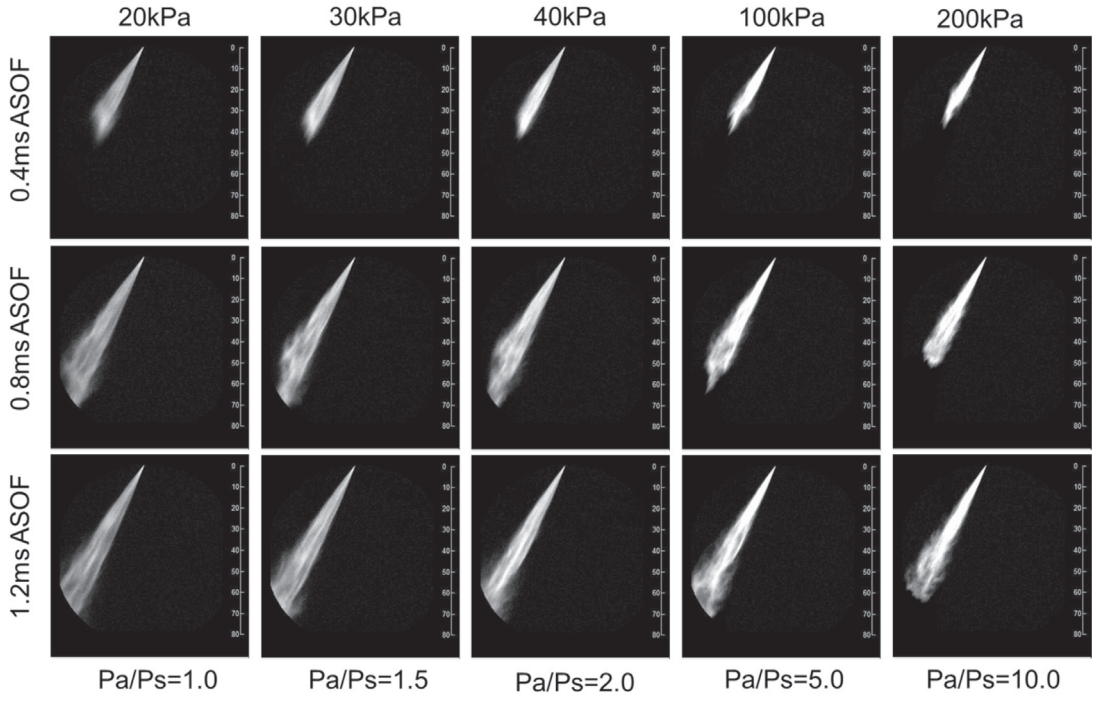

(a) Fuel temperature = 25 °C

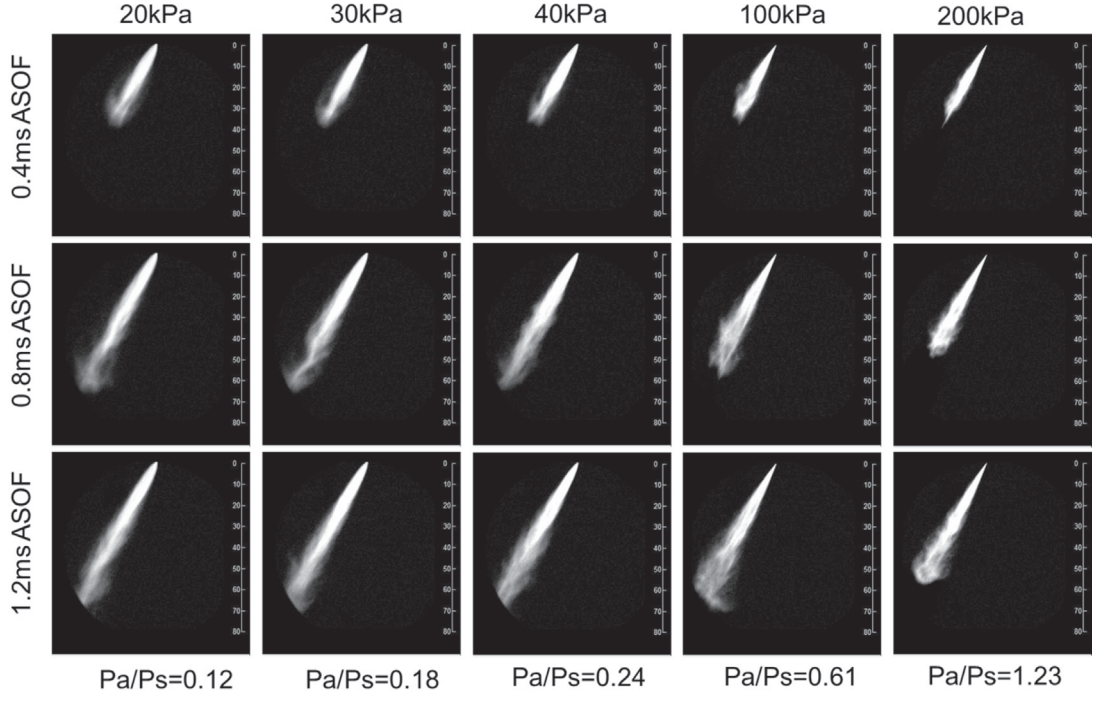

(b) Fuel temperature = 85 °C

Fig. 6. Spray imaging results for the 1-hole injector at lower (a) and higher (b) fuel temperatures and a range of ambient pressures. The dimensionless superheat degree, P_a/P_s, is provided below each column of images. The time after the start of injection (ASOF) for the images is provided to the left of each row.

promotes spray atomization and evaporation, and produces smaller fuel droplets, which can reduce spray penetration. Thus, the offsetting effects of stronger atomization caused by superheating (decreasing spray penetration) and lower air drag (increasing penetration) resulted in almost identical spray penetration for early times in the spray development for the higher fuel temperature.

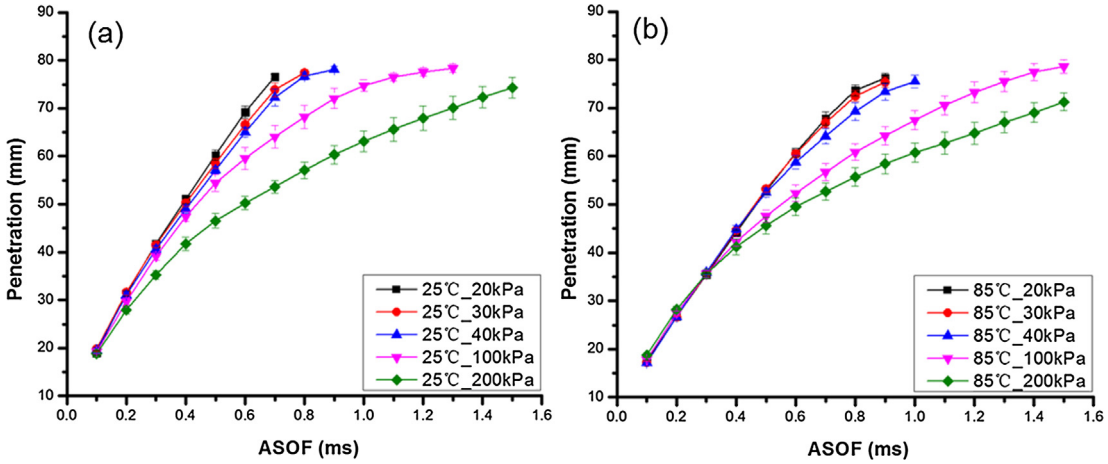

Fig. 7. Average spray penetration data as a function of time after the start of fuel injection for the 1-hole injector and the different fuel temperatures and ambient pressures. The error bars are the standard deviation of the 20 injection events.

3.2. Axial spray analysis of 6-hole injector

Fig. 8 shows spray image sequences of the 6-hole injector at the fuel temperatures of 25 °C and 85 °C, and ambient pressures from 20 kPa to 200 kPa. When the fuel temperature was 25 °C, typical spray structures of a multi-hole injector were observed. Individual fuel plumes could be identified, and no direct visible interactions between adjacent plumes were observed. Specifically, there was a clear gap between the plumes and the plumes appeared evenly distributed in space. The images of Fig. 8(a) show the fuel plumes were wider and penetrated faster with decreasing ambient pressure due to greater fuel atomization and smaller air drag forces at lower ambient pressures. When the fuel temperature was 85 °C, the spray structures change dramatically at the different ambient pressures, as seen in Fig. 8(b). When the ambient pressure was 200 kPa, the fuel was still subcooled, and the spray structure was similar to the structure observed when fuel the temperature was 25 °C. When the ambient pressure decreased to 100 kPa, slight plume interaction was observed between the central two plumes, but the fuel plumes still propagated in the direction oriented by the nozzle. Further decreasing the ambient pressure to 40 kPa and lower, significantly changed the spray characteristics. A collapsed spray structure with a longer and narrower spray was formed. With no gap between the central fuel plumes, the structure showed significant plume-to-plume interactions.

Fig. 9 shows the spray penetration as a function of injection time corresponding to the data presented in Fig. 8. As with the 1-hole injector, higher ambient pressure led to lower spray penetration for both fuel temperatures, even with the collapsed structures observed for the higher fuel temperature. For the higher fuel temperature, the slopes of the spray penetration curves are much larger at later times for the ambient pressures of 20 kPa, 30 kPa and 40 kPa compared with the slopes for the 100 kPa and 200 kPa conditions, which is attributed to the significant change of the spray structures at lower ambient pressures. A more detailed time sequence of the spray images for an ambient pressure of 40 kPa is shown in Fig. 10, and the images provide insight into the change in the rate of penetration. When the injection time was less than 0.8 ms ASOF, the spray tip was flat and vortices at the two sides of the spray tip were observed. Enhanced fuel atomization and air entrainment associated with the strong level of superheat at $P_a/P_s = 0.24$ resulted in short spray penetration. However, at 0.8 ms ASOF, a bulge appeared near the central region of the spray tip (highlighted by the arrow in Fig. 10). The bulge asymmetry appeared in all injection events studied at this condition. As the injection time continued, the bulge moved faster than the rest of the fluid at the spray tip, which dramatically increased the rate of spray penetration. This feature was only observed with the multi-hole injector is the source of the higher penetration seen in Fig. 9. Clearly, spray collapse has a remarkable impact on the spray structure of the multi-hole injector, and the features are not captured in the single-hole injector sprays.

Fig. 11 shows spray image sequences for 40 kPa and 100 kPa ambient pressures when the fuel temperature was 75 °C. The images show the spray structure collapsed when the ambient pressure was 40 kPa ($P_a/P_s = 0.33$), and the spray tip was almost flat at later times (e.g. 1 ms ASOF and later), without the bulge observed at the fuel temperature of 85 °C. For the ambient pressure of 100 kPa and fuel temperature of 75 °C, ($P_a/P_s = 0.82$) the spray did not collapse. Comparing the penetration at 1.5 ms ASOF (data not shown here), the 100 kPa spray was around 70 mm in length whereas the 40 kPa was approximately 60 mm. The results show that when spray collapse occurs but is not severe, spray penetration decreases.

To summarize, the imaging results show that when the fuel is superheated, interaction between the fuel plumes of a multi-hole injector occurs and leads to spray collapse. However, the extent of the spray collapse can have opposing effects on the spray. Slight spray collapse can result in shorter and wider sprays, while severe spray collapse can lead to much larger spray penetration and more concentrated or narrower fuel distribution. Understanding the mechanism of the spray collapse process of multi-hole injectors will clarify what controls the different characteristics and is discussed in the following sections.

3.3. Spray pattern analysis of the 6-hole injector

Fig. 12 shows the development of the spray patterns of the 6-hole injector taken at 40 mm downstream of the injector tip. The conditions for the experiments span P_a/P_s values from 0.12 to 2.0. When P_a/P_s was 2.0, the injection conditions were subcooled, and individual fuel plumes were clearly observed with no interaction between adjacent fuel plumes at any time. Furthermore, the spacing between the adjacent fuel plumes and the center of each plume remained constant throughout the spray event. When P_a/P_s was decreased to 0.44 by increasing the fuel temperature to 65 °C, plume interaction was observed after 1.0 ms ASOF, indicating the spray had individual plumes at injection times earlier than 1.0 ms ASOF (at the 40 mm cross-sectional plane). Interactions between adjacent plumes started near 1.2 ms ASOF for the 40 kPa ambient pressure and 65 °C fuel temperature condition, and eventually the fuel plumes formed a closed circular pattern after 1.7 ms ASOF. For the injection condition with the same P_a/P_s value of 0.44, but with a fuel temperature of 45 °C and ambient pressure of 20 kPa, plume interaction started earlier at 1.0 ms ASOF. Before 1.2 ms ASOF, the fuel of each plume was still concentrated around each plume center

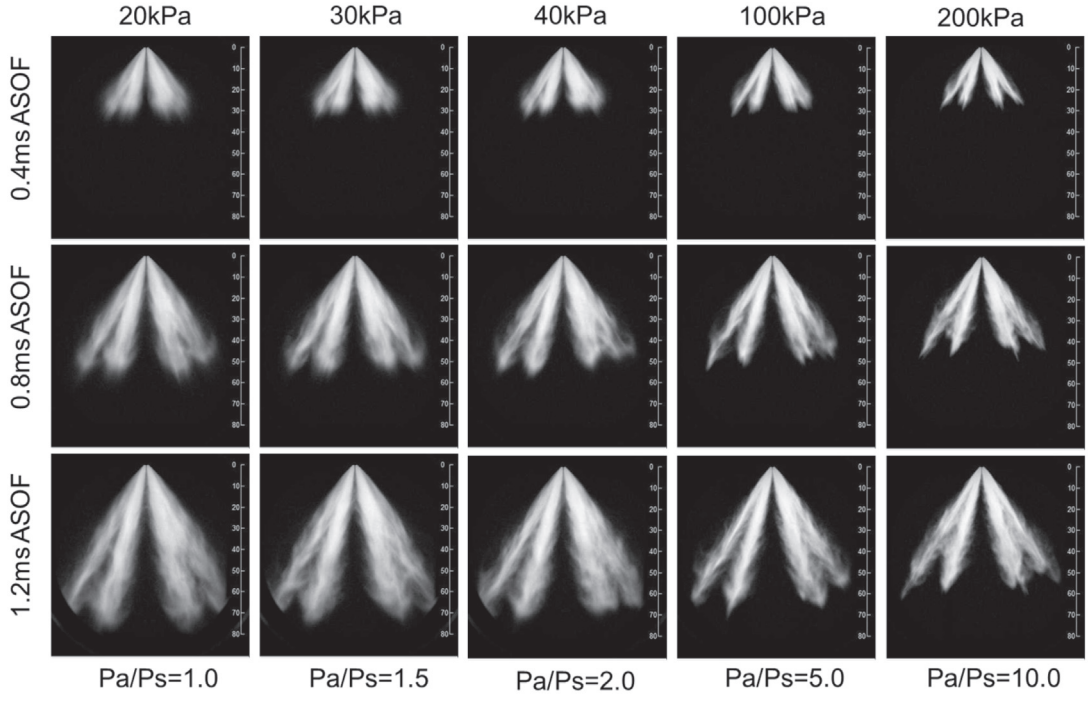

(a) Fuel temperature = 25 °C

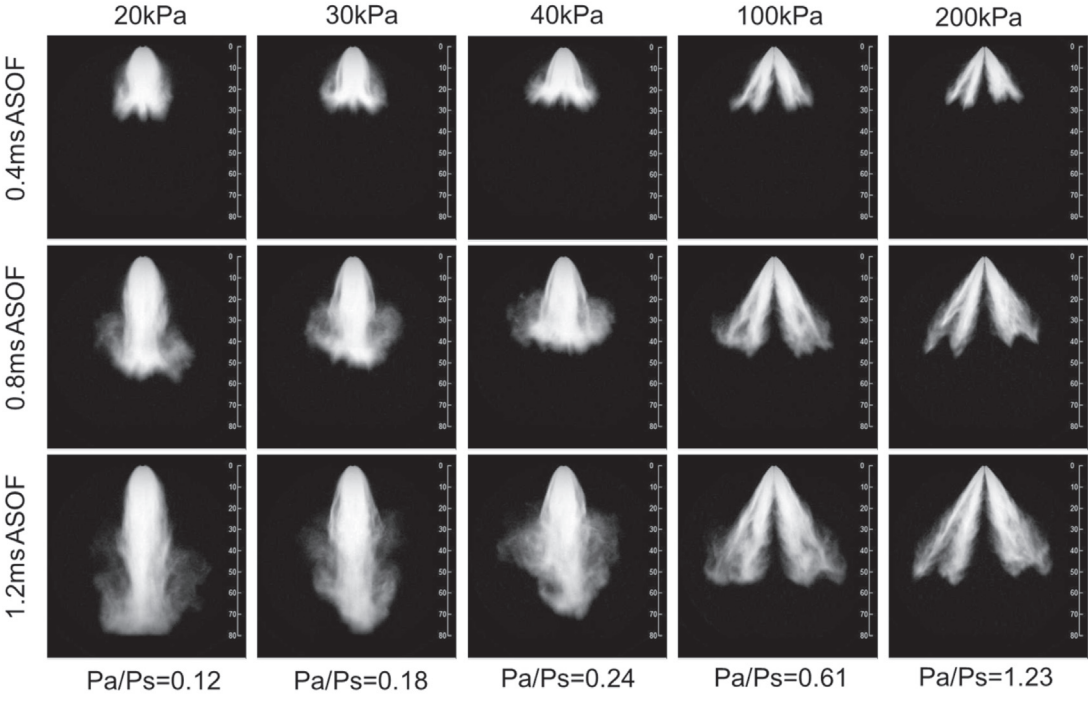

(b) Fuel temperature = 85 °C

Fig. 8. Spray imaging results for the 6-hole injector at lower (a) and higher (b) fuel temperatures and a range of ambient pressures. The dimensionless superheat degree, P_a/P_s, is provided below each column of images. The time ASOF is provided to the left of each row.

regardless of the slight plume interaction. In other words, the slight interaction between plumes had nearly no effect on fuel distribution before that time. After 1.2 ms ASOF, the fuel shifted to the center part of the spray with a significantly different fuel distribution, indicating spray collapse had occurred. The results show plume interaction and spray collapse need time to develop. Although the superheat degree was the same (P_a/P_s = 0.44), the processes of plume interaction and spray collapse were different, which indicates superheat degree which defines the thermal state of the fuel when it discharges into the chamber is important, but the absolute value of the ambient pressure also matters

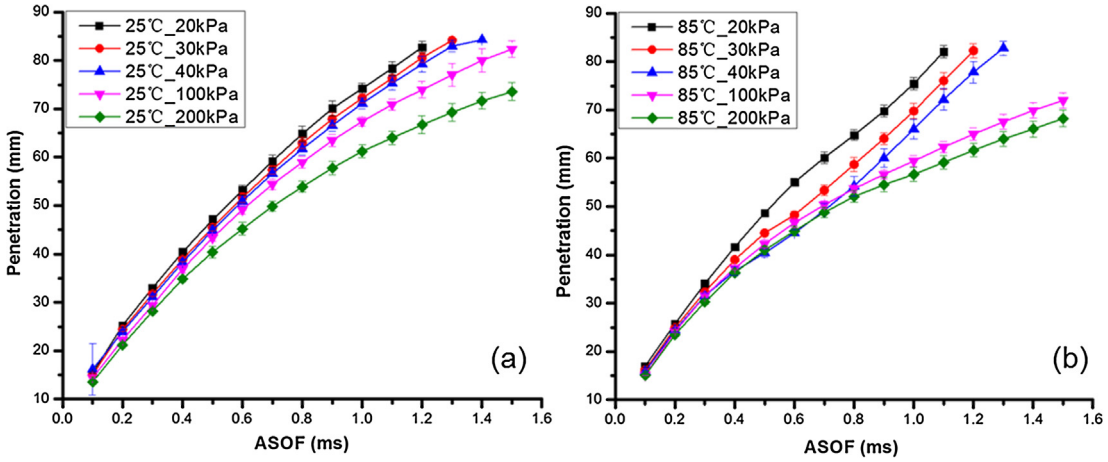

Fig. 9. Average spray penetration data as a function of time after the start of fuel injection for the 6-hole injector and the different fuel temperatures and ambient pressures. The error bars are the standard deviation of 20 injection events.

with respect to the spray collapse process. Lower ambient pressure results in earlier plume interaction and stronger spray collapse even when the P_a/P_s value is the same.

When P_a/P_s was decreased below 0.44, the start time of plume interaction shifted to earlier times. The earlier plume interaction resulted in more severely collapsed spray patterns, i.e. with fuel more concentrated at the center of the spray. When P_a/P_s was 0.22, severely collapsed spray patterns were observed, and at 2.0 ms ASOF, no liquid fuel could be seen at the center of the spray pattern. For P_a/P_s of 0.12, the smallest collapsed spray patterns were seen, with less liquid fuel at the spray center at 1.2 ms ASOF, and no liquid fuel observed at the center of the spray after 1.2 ms ASOF. Two explanations could be responsible for the observations. The fuel at the spray center could evaporate faster due to locally higher temperature and lower pressure [10] or the fuel cannot reach the spray center near the end of injection due to flow constraints.

Spray patterns at various cross-sectional planes are shown in Fig. 13 for conditions spanning P_a/P_s values from 0.12 to 2.0. The time offset between two sequential cross-sectional patterns was set as 0.2 ms for each incremental distance of 10 mm at each test condition. At subcooled conditions, namely $P_a/P_s = 2.0$, each individual fuel plume can be seen clearly even at the 10 mm cross-sectional plane. As fuel spray moved downward, the distance between adjacent fuel plumes increased due to the drill angle of each nozzle. When P_a/P_s was 0.46 or 0.44, plume interaction was identified close to the nozzle exit (by the 20 mm cross-sectional plane), but the fuel plumes were distinct again by the time the fuel spray reached the 40 mm and 60 mm cross-sectional planes. When P_a/P_s was 0.33, more severe interaction and spray collapse was seen at all planes, with the fuel concentrated at the center of the spray. However, the fuel dispersed more by the 40 mm cross-sectional plane, which indicated weaker plume interaction and weaker spray collapse for $P_a/P_s = 0.33$. At the 60 mm cross-sectional plane, strong fuel atomization and evaporation led to less liquid fuel in the images. When P_a/P_s was 0.3 and 0.12, the sprays were in the flare flash-boiling region, and more compact spray patterns and concentrated fuel distributions were observed at all test planes, indicating a stronger

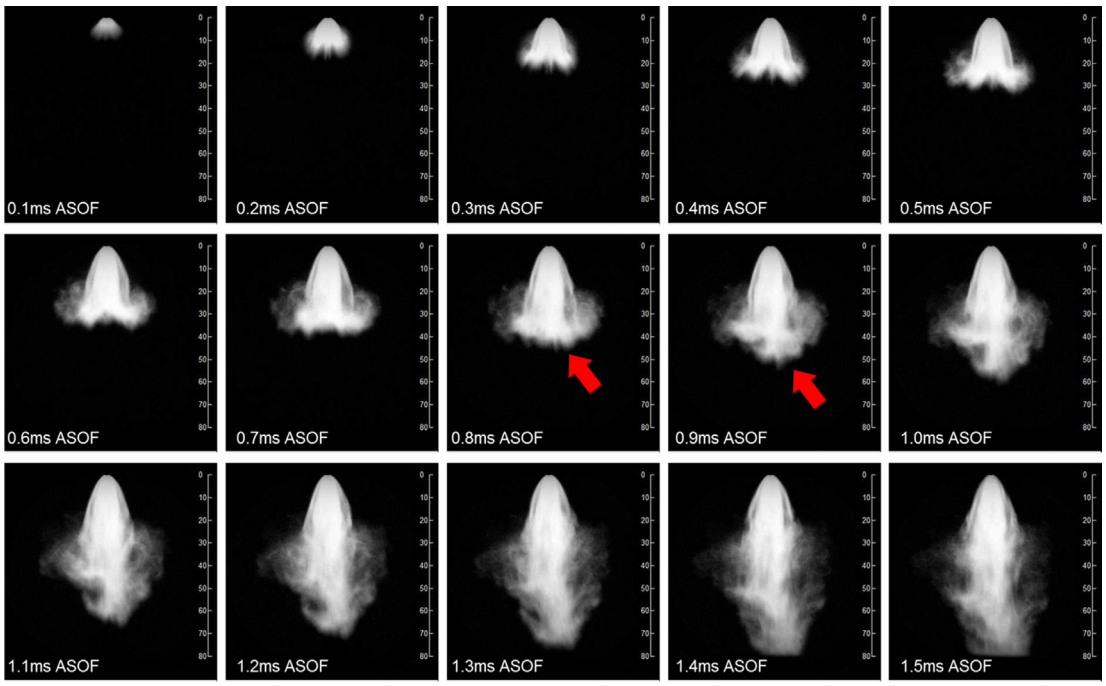

Fig. 10. Spray image sequence of the 6-hole injector for the fuel temperature of 85 °C, ambient pressure of 40 kPa, and $P_a/P_s = 0.24$. The arrow highlights the start of non-axisymmetric spray penetration.

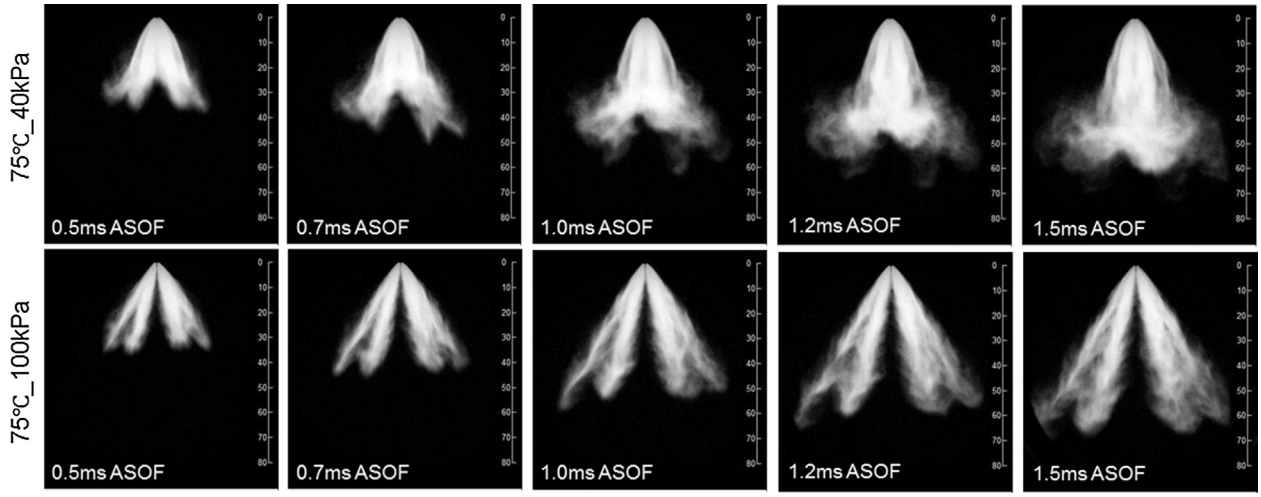

Fig. 11. Spray image sequences for fuel temperature of 75 °C and ambient pressures of 40 kPa (P_a/P_s = 0.33) and 100 kPa (P_a/P_s = 0.82).

collapse process. Overall, the spray pattern data show fuel plume interaction starts within the near nozzle region, and the visual liquid fuel interactions may continue or diminish as the fuel spray moves downward, and the extent of the interaction is dependent on the superheat degree.

Based on the spray pattern imaging data, the patterns can be divided into four categories, which are shown in Fig. 14. The first category is when no interaction occurs between fuel plumes, and all fuel plumes

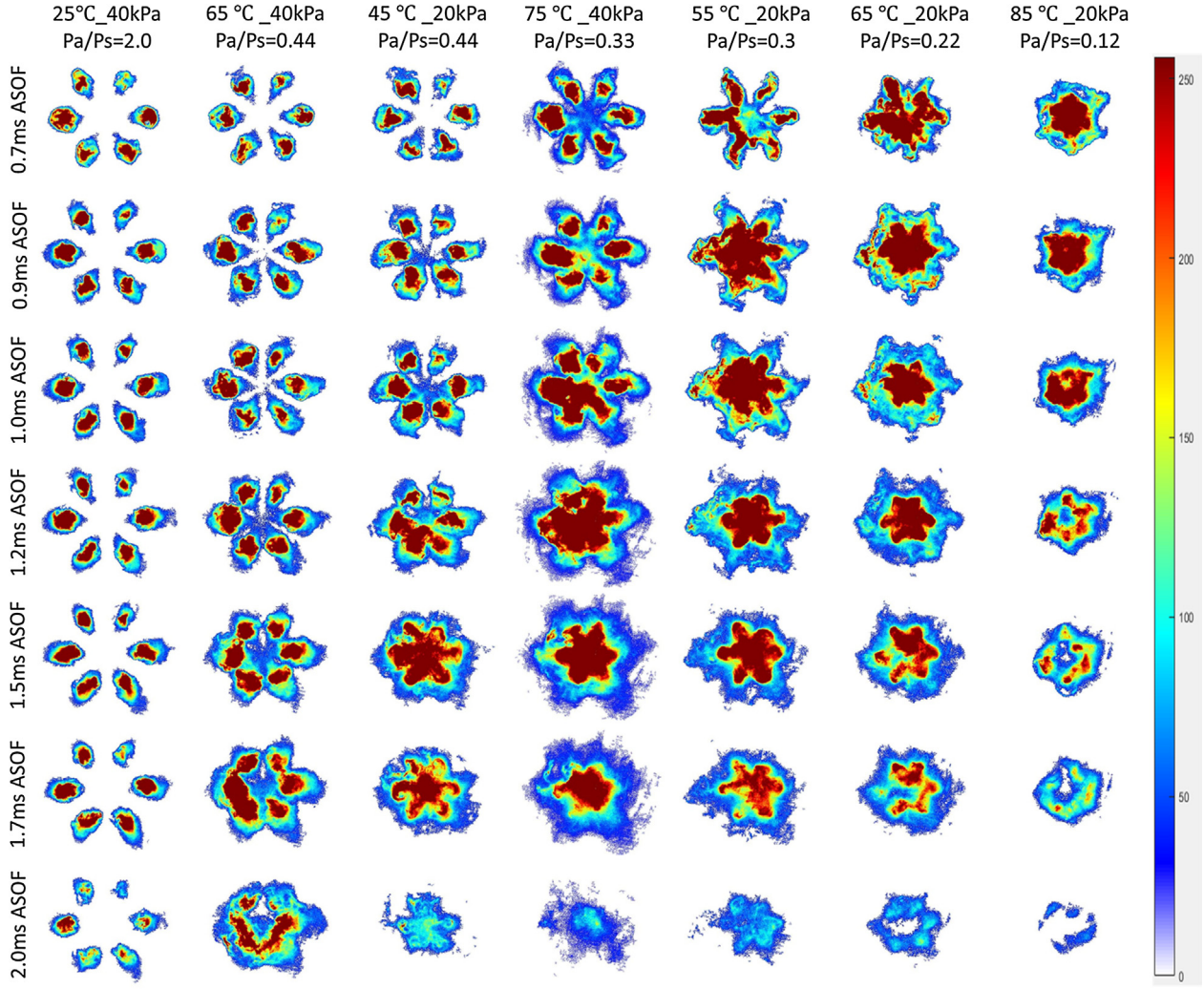

Fig. 12. Spray patterns as a function of time ASOF at 40 mm downstream of the injector tip of the 6-hole injector. The columns correspond to different fuel temperature, ambient pressure and dimensionless superheat degree, P_a/P_s, with P_a/P_s decreasing from left to right. The time ASOF is listed on the left of each row. The color scale (arbitrary units) indicates light intensity and corresponds to the presence of liquid fuel.

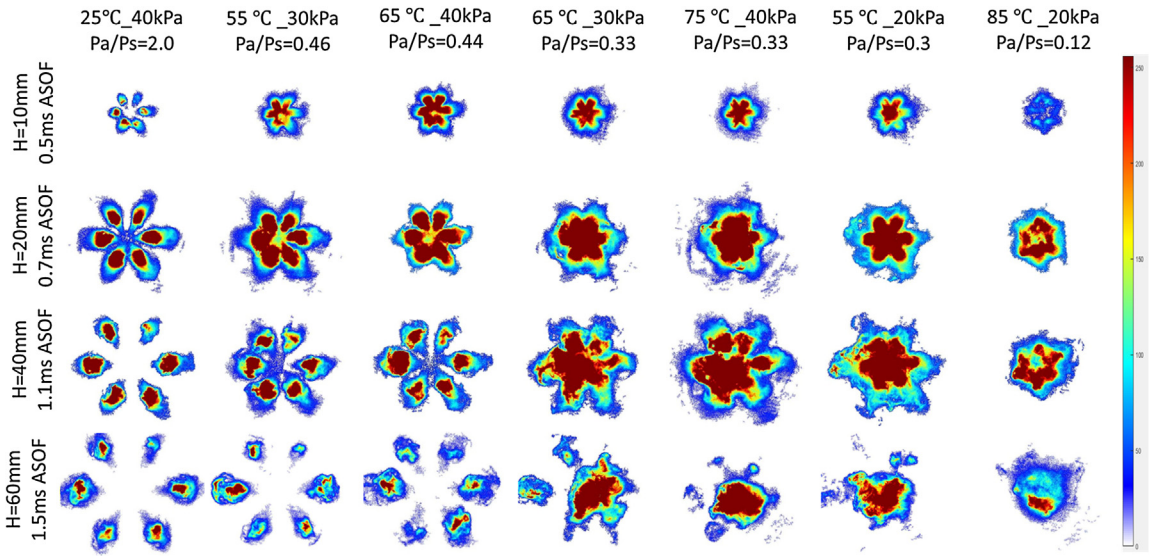

Fig. 13. Spray patterns at various cross-sectional planes downstream of the injector tip of the 6-hole injector. The columns correspond to different fuel temperature, ambient pressure and dimensionless superheat degree, P_a/P_s, with P_a/P_s decreasing from left to right. The time ASOF and H (the distance downstream of the injector tip) are provided to the left of each row. The color scale (arbitrary units) indicates light intensity and corresponds to the presence of liquid fuel.

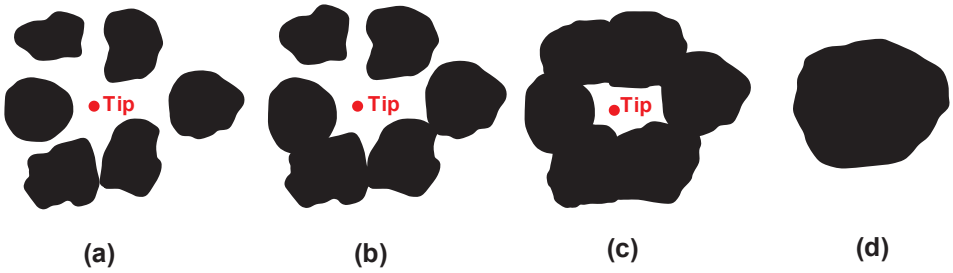

Fig. 14. Four categories of spray patterns proposed based on the observations of the current work. The progression from left to right qualitatively describes increasing plume interactions for a multi-hole fuel injector from no plume-to-plume interaction (a) to complete collapse of multiple plumes into one central structure (d).

propagate along the direction defined by the nozzle drill angles. The next category is when some interaction appears between some of the fuel plumes. Such slight plume interaction does not trigger any obvious transformation of the spray structure, like the trajectory of the plumes. The third category of spray pattern describes when all fuel plumes experience interactions and a closed region at the spray center appears. For this category, the nozzle configuration and the plume interactions affect the spray structure, but the nozzle configuration still plays the dominant role. For the last category, representing the strongest levels of superheating, the multiple fuel plumes merge into one plume due to spray collapse, and the spray collapse governs the spray structure, rather than the nozzle configuration as seen in this work and other previous studies of superheated/flash-boiling fuel sprays [25–27].

The four categories of spray patterns will induce different motion in the ambient gases surrounding the fuel spray. A schematic of proposed gas motion is illustrated in Fig. 15. In the figure, the suggested gas motion is highlighted by the arrows and the panels represent two distinct conditions. The first condition (corresponding to Fig. 14(a) and (b)) is when ambient air can be exchanged with the central region of the fuel spray, and the second condition (corresponding to Fig. 14(c) and (d)) is when the ambient air flow is obstructed from access to the central region of the spray. The momentum of the ambient gas is much smaller than the momentum of the fuel, so the air flow cannot change the fuel spray pattern. For conditions where the central region of the spray is inaccessible by the ambient air, the pressure in the center of the spray will decrease as the spray moves away from the injector. Eventually, the pressure differential between the surrounding ambient region and the spray center triggers severe collapse of the spray. Detailed analysis of this process can be found in Wu et al. [24]. For the spray structure shown on the right in Fig. 15, the severely collapsed spray would induce faster motion of the spray downward away from the nozzle exit, and result in longer penetration which is consistent with the observations seen in Fig. 10. For the spray structure shown on the left in Fig. 15, i.e. sprays where the ambient gases can be transported into the spray center, the air motion and mixing expands the width of the spray.

3.4. Analysis of the collapse mechanisms of flash-boiling sprays

There are two geometric parameters defined by the fuel spray that can be used to characterize the potential for fuel plume interactions. The development and definitions of the spray parameters are described here. Once the geometric spray parameters are defined, the effects of the injector design and operating conditions are discussed in terms of the impact on the spray development and potential for increasing or decreasing plume interaction as observed in the current work and in other studies of spray collapse in the literature.

Fig. 16 is a schematic of the axial and radial spray structures of a 6-hole injector. The six holes are symmetrically distributed around the center of the injector tip. The drill angle of each nozzle is θ, and the number of holes is n, where n is six for the injector used in this work. Key dimensions are defined in Fig. 16. For a given distance H downstream of the injector tip, the distance from the plume centerline and the injector centerline, R, is

$$R = H * \tan\theta \quad (1)$$

On the cross-sectional plane, which is the distance H downstream of

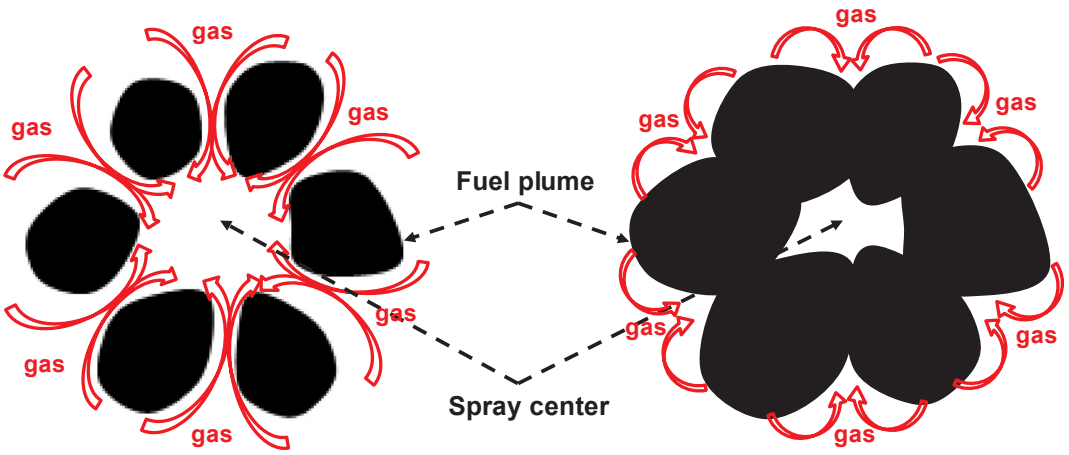

(a) Spray pattern

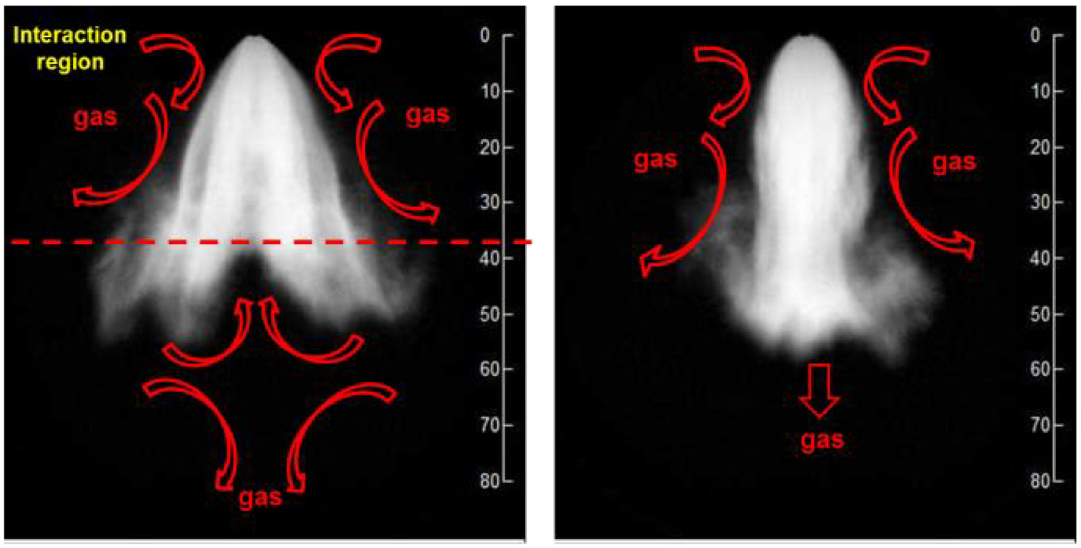

(b) Axial spray structure

Fig. 15. Sketches indicating the different air motion induced by the different categories of spray patterns (a) and spray structures (b). The panels on the left show the motion when ambient air can be exchanged with the air at the center of the spray. The panels on the right show the motion when ambient air cannot access the center region of the spray.

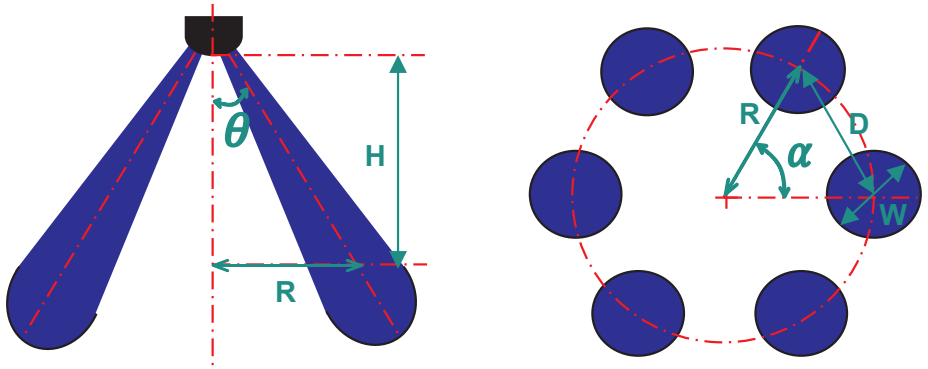

(a) axial spray structure (b) radial spray structure

Fig. 16. Illustration of the spray structure of a multi-hole injector.

the injector tip, the angle between two adjacent fuel plumes, α, is

$$\alpha = 2\pi/n \tag{2}$$

The distance between the center points of two adjacent fuel plumes at the H cross-sectional plane, $D(H)$, is

$$D(H) = 2R * \sin(\alpha/2) = 2R * \sin(\pi/n) \tag{3}$$

Substituting Eq. (1) into Eq. (3) yields

$$D(H) = 2H * \tan\theta * \sin(\pi/n) \tag{4}$$

Thus the distance between two plumes, $D(H)$, is a function of the nozzle configuration (i.e. the drill angle of the nozzle), and is independent of injection time and other injection parameters.

The width of a single fuel plume at the H cross-sectional plane at injection time t is $W(H, t)$, and is influenced by superheat degree, the ratio of ambient gas density to fuel density, nozzle diameter, fuel Reynolds number and so on. If $W(H, t) < D(H)$, i.e., the distance between two adjacent fuel plumes is larger than the plume width, there is no visible interaction between the two plumes. If $W(H, t) = D(H)$, i.e., the distance between two adjacent fuel plumes is equal to the plume width, visible plume interaction occurs. Assuming the fuel plumes start interacting at injection time t_1 at the H_1 cross-sectional plane, then$W(H_1, t_1) = D(H_1)$.

Because the holes are symmetrically distributed around the nozzle tip, when each plume is just touching, the spray can generate a continuous spray pattern similar to that shown in Fig. 14(c). As the spray develops and moves downward, at injection time of t_2 at the H_2 cross-sectional plane, the plume width is $W(H_2, t_2)$ and the distance between adjacent fuel plumes is $D(H_2)$. So the change in the distance between two adjacent fuel plumes ΔD is

$$\Delta D = D(H_2) - D(H_1) = 2 * \Delta H * \tan\theta * \sin(\pi/n) \tag{5}$$

where, $\Delta H = H_2 - H_1$, which is always positive. Thus, ΔD is always positive, which indicates that as the spray moves downward, the fuel plumes will have the tendency to separate or move further apart. Larger nozzle drill angles or fewer nozzles would lead to larger ΔD. However, the fuel plumes will also atomize and expand, which results in wider fuel plumes. The change in the plume width at the H_2 cross-sectional plane at the injection time of t_2 is ΔW:

$$\Delta W = W(H_2, t_2) - W(H_1, t_1) \tag{6}$$

and ΔW is governed by the atomization process of the fuel plumes.

If the plumes are just touching at time t_1, whether the spray interaction continues or ceases at a later injection time t_2 (at the H_2 cross-sectional plane) depends on the change in the spacing between the plumes, ΔD, and the change in the width of the plumes, ΔW. If $\Delta D > \Delta W$, i.e., the change in the distance between adjacent fuel plumes is larger than the change in the plume width, the fuel plumes separate. This behavior can be observed in the near nozzle region. For example in Fig. 13 for the conditions of 55 °C and 30 kPa ($P_a/P_s = 0.46$), the plumes were initially touching at H = 10 mm and H = 20 mm, but the plumes separated as the spray developed and moved downward at H = 60 mm. If $\Delta D < \Delta W$, or the change in the distance between adjacent fuel plumes was smaller than the increment of change in the plume width, the fuel plumes would continue to interact. This situation is consistent with the collapsed spray pattern observed in Fig. 13 for the conditions of 55 °C and 20 kPa ($P_a/P_s = 0.30$).

In addition to the nozzle physical configuration, external effects like the motion of the ambient gas can influence the fuel plume interactions. For these conditions, ΔD at the injection time of t_2 should be modified by introducing a factor to correct for the effects of ambient gas motion and the low pressure at the center of the spray. So Eq. (5) becomes:

$$\Delta D = 2 * \Delta H * \tan\theta * \sin\left(\frac{\pi}{n}\right) - \delta \tag{7}$$

where δ is the change in the distance between adjacent fuel plumes caused by ambient gas motion, pressure differentials between the interior and exterior regions of the spray surface, etc. δ is always positive, because ambient gas motion and other similar effects would reduce the distance between adjacent fuel plumes. For these conditions, the fuel plumes would continue to interact as the spray develops and moves downward. The effects of the external motion explains why fuel plumes do not interact at early injection times, but do interact as the spray develops as seen in Fig. 12 for conditions of 45 °C and 20 kPa ($P_a/P_s = 0.44$). As the superheat degree decreases, fuel atomization increases and the effects of ambient gas motion and therefore δ increase. Thus, ΔD decreases which leads to severely collapsed spray structures, as seen in Fig. 8(b) for conditions of 85 °C 30 kPa ($P_a/P_s = 0.18$) and Fig. 13 for conditions of 55 °C and 20 kPa ($P_a/P_s = 0.3$).

3.5. Consideration of parameters affecting collapse of flash-boiling sprays

A key outcome of the analysis of the spray features is the comparison between the change in the distance between adjacent fuel plumes and the change in the width of the fuel plumes as the spray develops. Thus, to understand the effects of injection parameters (like hardware configuration and operating conditions) on spray collapse, consideration of how the injection parameters affect *D, W, ΔD* and *ΔW* provides a means to interpret the results of the current work and previous studies of fuel spray collapse in the literature.

3.5.1. Injector configuration

Hardware characteristics of GDI injectors that affect the spray characteristics include the nozzle diameter, length, and drill angle and the number of nozzles. Nozzle diameter and length can influence the internal flow and subsequently the spray characteristics. For example, adjusting the nozzle diameter and length can improve in-nozzle flow turbulence and the radial velocity component, and the plume width would be expected to increase. For a fixed nozzle diameter, increasing the nozzle length from a small value to a large value, the flow turbulence would first increase with increasing nozzle length, and then decrease with increasing nozzle length [43]. Flash-boiling effects also have to be considered when changing nozzle diameter and length. For example, a longer nozzle length has enhanced wall restriction effects, which would reduce in-nozzle flow turbulence and lead to a narrower fuel plume [16,17,44]. However, a longer nozzle length would also produce more flash-boiling bubbles along the nozzle wall, which promotes spray atomization significantly and therefore would be expected to increase plume width. Due to these potentially offsetting effects, there is no unique trend on how nozzle diameter and length influence plume width.

The effects of the other nozzle hardware characteristics are clearer. More nozzles would decrease the distance between adjacent fuel plumes, enabling and increasing the potential for plume interactions and spray collapse. For example, Aori et al. [45] found a 6-hole injector exhibited more collapsed fuel spray structure at flash-boiling conditions than a 5-hole injector and a 4-hole injector. Larger nozzle drill angles produce not only larger distances between adjacent fuel plumes (*D*), but also larger changes in the distance between fuel plumes (*ΔD*), which suppresses plume interaction and spray collapse, as found by Mojtabi et al. [33], where fuel spray of an injector with a 60° nominal angle underwent more severe collapse behavior than the fuel spray of an injector with a 90° nominal angle.

3.5.2. Fuel pressure

Higher fuel pressure can promote fuel atomization due to stronger fuel turbulence and air drag forces which could expand the fuel plumes. However, higher fuel pressure also increases the fuel velocity, and consequently leads to higher momentum of the fuel droplets. The higher velocity of the fuel droplets reduces the time to transit from the H_1 cross-sectional plane to the H_2 cross-sectional plane, giving the fuel plume less time to expand. On the other hand, fuel droplets with higher

momentum are less influenced by the motion of the ambient gas, which means δ would be smaller. Which process dominates will depend on the specific operating conditions and injector design. In Schulz and Beyrau [29], the authors found more collapsed spray patterns using 150 bar fuel pressure compared with using 300 bar fuel pressure, indicating the momentum effects were stronger than the mixing effects. Chan et al. [26] also found increasing injection pressure reduced collapse of flash-boiling spray in an optical SIDI engine. Jiang et al. [34] found that higher injection pressure led to a longer distance before spray eventually collapsed.

3.5.3. Fuel properties

Fuel properties can affect in-nozzle flow characteristics, spray breakup and dispersion processes. Central to spray behavior are fuel density, viscosity, surface tension and boiling point. Fuels with higher densities result in smaller plume angles according to the empirical expressions derived for diesel and gasoline sprays in Refs. [46–49]. Higher fuel density leads to higher momentum of the fuel droplets, thus reducing the effects of the ambient gas on the spray, i.e., smaller δ. Fuel density and dynamic viscosity both affect the spray Reynolds number, which affects fuel and air mixing and spray breakup. Depending on the effects on Reynolds number, W and ΔW could decrease with reduced Reynolds number, suppressing plume interaction and the collapse process. Higher fuel surface tension could decrease the rate of droplet breakup, decreasing W and ΔW. In addition, higher surface tension makes initiation and growth of flash-boiling bubbles in the liquid fuel more difficult, which decreases spray atomization. The fuel boiling point plays the most vital role among the fuel properties at flash-boiling conditions. Lower boiling point increases the level of fuel superheat for a fixed fuel temperature, which promotes fuel atomization and evaporation significantly. Stronger superheated conditions will result in wider fuel plumes and larger changes in plume width, thus enhancing plume interaction and spray collapse.

3.5.4. Ambient state conditions

Ambient gas density, pressure and temperature are the main parameters influencing fuel spray characteristics. Higher ambient gas density produces larger air drag forces, which promote spray breakup and reduce the velocity of the fuel spray [49]. In addition, some empirical expressions for fuel plume angle for diesel and gasoline sprays [44,46–49] indicate higher ambient density results in larger plume angle. Therefore, higher ambient gas density can promote plume interaction and spray collapse.

Ambient pressure governs the state of the fuel after it is discharged from the nozzle. Lower ambient pressure produces higher levels of superheat, which results in larger W and ΔW, enhancing fuel plume interaction and spray collapse as observed in this work. Higher ambient gas temperatures can heat the fuel spray and improve fuel evaporation resulting in lower W and ΔW and thereby mitigating plume interaction and collapse. In the study by Park et al. [50], using both experimental and numerical methods, higher ambient gas temperatures led to smaller cone angles and higher spray penetration. Pan et al. [51] also found that fuel plume was slightly smaller with enhanced evaporation at higher ambient temperatures, which has the potential to reduce plume interaction and spray collapse.

Overall, which characteristics are the most critical to controlling the spray collapse process depends on the relative magnitude of the effects of these different parameters. At some operating conditions, one category can dominate, like the ambient state conditions or the fuel injector hardware configuration.

4. Conclusions

An experimental investigation of two GDI injectors (a single hole and a 6-hole) was conducted under a wide range of sub-cooled and superheated conditions. Both axial and radial macroscopic spray structures were recorded and analyzed. The key conclusions of the study are:

1) For the 1-hole injector, decreasing ambient pressure did lead to flash-boiling sprays, and consequently enhanced fuel atomization; however, spray penetration was primarily influenced by the ambient gas density. Lower ambient pressure decreased the ambient gas density, and increased the rate of spray penetration and flash boiling did not change the trajectory of the fuel plume. Ultimately, however, the spray processes important with a multi-hole injector are not well represented by a single-hole injector when considering the spray collapse process. Plume interaction is critical to describing the potential for spray collapse.
2) For the 6-hole injector at flash-boiling conditions, the adjacent fuel plumes interacted with each other. Slight plume interactions did not significantly affect the spray structure, but could reduce the spray penetration rate and increase the spray angle. Strong plume interactions triggered severe spray collapse, which altered the spray structure significantly and resulted in longer spray penetration and smaller spray angle.
3) Interaction of adjacent fuel plumes often started in the near nozzle region, and whether the interactions continued or ceased as the spray developed and moved downward was mainly dependent on the injector configuration and superheat degree. At strong flash-boiling conditions ($P_a/P_s < 0.3$), plume interaction increased with injection time for the multi-hole injector studied.
4) Differences in air motion triggered by plume interactions is suggested as the primary cause of the severely collapsed spray structures observed, where multiple plumes merged into one continuous surface and produced a longer and narrower fuel spray structure.
5) The nozzle hardware configuration and injection parameters dictate the level of fuel plume interaction and the potential transition to spray collapse. Adjusting parameters that can increase the distance between adjacent fuel plumes or reduce the plume width, can suppress plume interaction and the spray collapse process and vice versa.

Acknowledgement

Experiments in this study were conducted at the National Engineering Laboratory for Automotive Electronic Control Technology of Shanghai Jiao Tong University. The authors acknowledge hardware and technical support from GM R&D in the USA and GM China.

References

[1] Senda J, Wada Y, Kawano D, Fujimoto H. Improvement of combustion and emissions in diesel engines by means of enhanced mixture formation based on flash boiling of mixed fuel. Int J Engine Res 2008;9:15–27.
[2] She JP. Experimental study on improvement of diesel combustion and emissions using flash boiling injection. SAE Technical Paper 2010; 2010-01-0341.
[3] Xu M, Hung D, Yang J, Wu S. Flash-boiling spray behavior and combustion in a direct injection gasoline engine. Proceedings of the Australian Combustion Symposium, Melbourne, Australian, 2015, Sep.
[4] Yang J, Dong X, Wu Q, Xu M. Influence of flash boiling spray on the combustion characteristics of a spark-ignition direct-injection optical engine under cold start. Combust Flame 2018;188:66–76.
[5] Xu M, Zhang Y, Zeng W, Zhang G, Zhang M. Flash boiling: easy and better way to generate ideal sprays than the high injection pressure. SAE Int J Fuels Lubr 2013;6:137–48.
[6] Zeng W, Xu M, Zhang Y, Wang Z. Laser sheet dropsizing of evaporating sprays using simultaneous LIEF/MIE techniques. Proc Combust Inst 2013;34(1):1677–85.
[7] Shen S, Jia M, Wang T, Lü Q, Sun K. Measurement of the droplets sizes of a flash boiling spray using an improved extended glare point velocimetry and sizing. Exp Fluids 2016;57:56.
[8] Adachi M, McDonell V, Tanaka D, Senda J, Fujimoto H. Characterization of fuel vapor concentration inside a flash boiling spray. SAE Technical Paper 1997; 970871.
[9] Zhang G, Xu M, Zhang Y, Zhang M, Cleary D. Macroscopic characterization of flash-boiling multi-hole sprays using planar laser induced exciplex fluorescence technique Part I. On-axis spray structure. Atomiz Sprays 2012;22(10):861–78.

[10] Zhang G, Hung D, Xu M. Experimental study of flash boiling spray vaporization through quantitative vapor concentration and liquid temperature measurements. Exp Fluids 2014;55(8):1804.

[11] Li T, Xu M, Wu S, Xu Q, Hung DL. Influence of the injector configuration on the spray evaporation characteristics under superheated conditions. SAE Technical Paper 2015; 2015-01-1900.

[12] Wu S, Xu M, Hung DL, Li T, Pan H. Analyzing the cycle-to-cycle variations of vapor and liquid phases of evaporating SIDI sprays via proper orthogonal decomposition technique. SAE Int J Engines 2015;9(1):193–200.

[13] Zhang M, Xu M, Hung DL. Simultaneous two-phase flow measurement of spray mixing process by means of high-speed two-color PIV. Meas Sci Technol 2014;25(9):095204.

[14] Park BS, Lee SY. An experimental investigation of the flash atomization mechanism. Atom Sprays 1994;4(2):159–79.

[15] Günther A, Wirth K. Evaporation phenomena in superheated atomization and its impact on the generated spray. Int J Heat Mass Transf 2013;64:952–65.

[16] Wu S, Xu M, Hung D, Pan H. In-nozzle flow investigation of flash boiling fuel sprays. Appl Therm Eng 2017;117:644–51.

[17] Wu S, Xu M, Hung D, Pan H. Effects of nozzle configuration on internal flow and primary jet breakup of flash boiling fuel sprays. Int J Heat Mass Transf 2017;110:730–8.

[18] Serras-Pereira J, Van Romunde Z, Aleiferis PG, Richardson D, Wallace S, Cracknell RF. Cavitation, primary break-up and flash boiling of gasoline, iso-octane and n-pentane with a real-size optical direct-injection nozzle. Fuel 2010;89(9):2592–607.

[19] Aleiferis PG, van Romunde ZR. An analysis of spray development with iso-octane, n-pentane, gasoline, ethanol and n-butanol from a multi-hole injector under hot fuel conditions. Fuel 2013;105:143–68.

[20] Wang B, Wang Z, Bao X, Li Y, Jiang Y, Xu H, et al. Microscopic investigation of near-field spray characteristics of 2-methylfuran, ethanol and isooctane under flash boiling conditions. Fuel 2018;215:142–52.

[21] Alghamdi T, Thoroddsen ST, Hernández-Sánchez JF. Ultra-high speed visualization of a flash-boiling jet in a low-pressure environment. Int J Multiph Flow 2019;110:238–55.

[22] Li T, Xu M, Hung D, Wu S, Cheng S. Understanding the effects of fuel type and injection conditions on spray evaporation using optical diagnostics. SAE Technical Paper 2015; 2015-01-0926.

[23] Kale R, Banerjee R. Experimental investigation on GDI spray behavior of isooctane and alcohols at elevated pressure and temperature conditions. Fuel 2019;236:1–12.

[24] Wu S, Xu M, Hung DL, Li T, Pan H. Near-nozzle spray and spray collapse characteristics of spark-ignition direct-injection fuel injectors under sub-cooled and superheated conditions. Fuel 2016;183:322–34.

[25] Zeng W, Xu M, Zhang G, Zhang Y, Cleary DJ. Atomization and vaporization for flash-boiling multi-hole sprays with alcohol fuels. Fuel 2012;95:287–97.

[26] Chan Q, Bao Y, Kook S. Effects of injection pressure on the structural transformation of flash-boiling sprays of gasoline and ethanol in a spark-ignition direct-injection (SIDI) engine. Fuel 2014;130:228–40.

[27] Guo H, Ding H, Li Y, Ma X, Wang Z, Xu H, et al. Comparison of spray collapses at elevated ambient pressure and flash boiling conditions using multi-hole gasoline direct injector. Fuel 2017;199:125–34.

[28] Lacey J, Poursadegh F, Brear MJ, Gordon R, Petersen P, Lakey C, et al. Generalizing the behavior of flash-boiling plume interaction and spray collapse for multi-hole direct injection. Fuel 2017;200:345–56.

[29] Schulz F, Beyrau F. The influence of flash-boiling on spray-targeting and fuel film formation. Fuel 2017;208:587–94.

[30] Zhang G, Xu M, Zhang Y, Hung D. Characteristics of flash boiling fuel sprays from three types of injector for spark ignition direct injection (SIDI) engines. In: Proceedings of the FISITA 2012 world automotive congress 2013; 443–454.

[31] Wu S, Pan H, Xu M, Hung D, Li T. Investigation of rapid atomization and collapse of superheated liquid fuel spray under superheated conditions. Atom Sprays 2016;26(12):1361–84.

[32] Wu S, Meinhart M, Yi J. Split injection spray characterization of three different types of GDI injectors at various fuel temperatures. In: 14th Triennial International Conference on Liquid Atomization and Spray Systems, Chicago, IL, USA, 2018, July 22–26.

[33] Mojtabi M, Chadwick N, Wigley G, Helie J. The effect of flash boiling on breakup and atomisation in GDI sprays. In: Proceedings of the 22nd European Conference on Liquid Atomization and Spray Systems. ILASS Europe. Como Lake, Italy, 2008 Sep. 08–10.

[34] Jiang C, Parker MC, Helie J, Spencer A, Garner CP, Wigley G. Impact of gasoline direct injection fuel injector hole geometry on spray characteristics under flash boiling and ambient conditions. Fuel 2019;241:71–82.

[35] Li Y, Guo H, Fei S, Ma X, Zhang Z, Chen L, et al. An exploration on collapse mechanism of multi-jet flash-boiling sprays. Appl Therm Eng 2018;134:20–8.

[36] Liao Y, Lucas D. Computational modelling of flash boiling flows: a literature survey. Int J Heat Mass Transf 2017;111:246–65.

[37] Zeng Y, Lee CFF. An atomization model for flash boiling sprays. Combust Sci Technol 2001;169(1):45–67.

[38] Kawano D, Goto Y, Odaka M, Senda J. Modeling atomization and vaporization processes of flash-boiling spray. SAE Technical Paper 2004; 2004-01-0534.

[39] Moulai M, Grover R, Parrish S, Schmidt D. Internal and near-nozzle flow in a multi-hole gasoline injector under flashing and non-flashing conditions. SAE Technical Paper 2015; 2015-01-0944.

[40] Saha K, Som S, Battistoni M, Li Y, Quan S, Senecal P. Modeling of internal and near-nozzle flow for a gasoline direct injection fuel injector. J Energy Res Technol 2016;138(5):052208.

[41] Saha K, Battistoni M, Som S. Modeling of flash boiling phenomenon in internal and near-nozzle flow of fuel injectors. Droplets and sprays. Singapore: Springer; 2018. p. 167–81.

[42] Hiroyasu H, Arai M. Structures of fuel sprays in diesel engines. SAE Technical Paper 1990; 900475.

[43] Birouk M, Lekic N. Liquid jet breakup in quiescent atmosphere: a review. Atom Sprays 2009;19(6):501–28.

[44] Wu S, Xu M, Yang S, Yin P. Contrary effects of nozzle length on spray primary breakup under subcooled and superheated conditions. SAE Technical Paper 2018; 2018-01-0302.

[45] Aori G, Hung D, Zhang M, Zhang G, Li T. Effect of nozzle configuration on macroscopic spray characteristics of multi-hole fuel injectors under superheated conditions. Atom Sprays 2016;26(5):439–62.

[46] Ranz W. Some experiments on orifice sprays. Canadian J Chem Eng 1958;36(4):175–81.

[47] Naber J, Siebers D. Effects of gas density and vaporization on penetration and dispersion of diesel sprays. SAE Technical Paper 1996; 960034.

[48] Zhang G, Xu M, Li T, Grover R, Kuo T, He Y. A study of near-field spray structure under superheated conditions of a gasoline fuel spray. In: The 26th annual conference on liquid atomization and spray systems-Americas, Portland, OR, USA, 2014 May 18–21.

[49] Huang W, Wu Z, Li L, Hu Z, Gao Y, Deng J. Effect of ambient density and temperature on diesel spray characteristics. SAE Technical Paper 2014; 2014-01-1414.

[50] Park S, Kim H, Lee C. Comparison of experimental and predicted atomization characteristics of high-pressure diesel spray under various fuel and ambient temperature. J Mech Sci Technol 2010;24:1491.

[51] Pan H, Xu M, Hung D, Wu S, Gu P, Dong X. Effect of ambient temperature on spray structure and evaporation of liquid spray and flash-boiling spray. Busan, Korea: FISITA; 2016. p. 26–30.